Interdecadal Pacific Oscillation responsible for the linkage of decadal changes in precipitation/moisture in arid central Asia and humid Asian monsoon region during the last millennium

Hongna Xu[1], Tao Wang[1,2,*], Huijun Wang[1,2]

[1] Collaborative Innovation Center on Forecast and Evaluation of Meteorological Disasters (CIC-FEMD), Nanjing University of Information Science and Technology, Nanjing 210044, China

[2] Climate Change Research Center and Nansen-Zhu International Research Centre, Institute of Atmospheric Physics, Chinese Academy of Sciences, Beijing 100029, China

* Corresponding author: Tao Wang (wangtao@mail.iap.ac.cn)

Abstract

Reconstruction and observational studies imply a potential linkage of moisture/precipitation change in arid central Asia and monsoonal East Asia, in which the evolution of moisture/precipitation in central Asia is out-of-phase with that in northern China, but in-phase with that in southern China. In order to ascertain whether there is a robust linkage between the changes in climate in Asian arid regions and monsoon regions and to elucidate the underlying dynamic mechanisms, we analyzed the Last Millennium Reanalysis dataset and outputs from the Community Earth System Model-Last Millennium Ensemble (CESM-LME). The results indicate a significant decadal linkage between precipitation changes in central Asia's arid region and the Asian monsoon region during the last millennium, which is primarily driven by the Interdecadal Pacific Oscillation (IPO). In spring, the positive IPO could enhance westerlies over the Mediterranean Sea and to its east, which could transport more water vapor and cause increased precipitation over central Asia. In summer, the positive IPO is accompanied with weakened Asian monsoon and southward Asian subtropical westerly jet, which can lead to increased (decreased) summer precipitation over southern China (over northern China and South Asia). The IPO plays a dominant role in connecting the decadal variations in precipitation between arid central Asia and monsoonal Asia by modulating the precipitation of their respective major rainy seasons. Model results suggest that this decadal linkage stems entirely from the internal variability present in the CESM-LME control and all single-forcing simulations. Changes in external forcing factors do not alter this inherent linkage

36 caused by IPO. Moreover, based on analyses of the aridity index and soil moisture

37 content, this relationship of precipitation variation also causes a similar decadal

38 linkage of moisture changes in central Asia and monsoonal Asia. The differences in

39 the multi-centennial-scale moisture/precipitation variations in the Asian arid region

40 and the monsoon region between the Medieval Climate Anomaly and Little Ice Age

41 are also likely caused by IPO-like sea surface temperature anomalies.

42 **Graphical abstract**

43

44
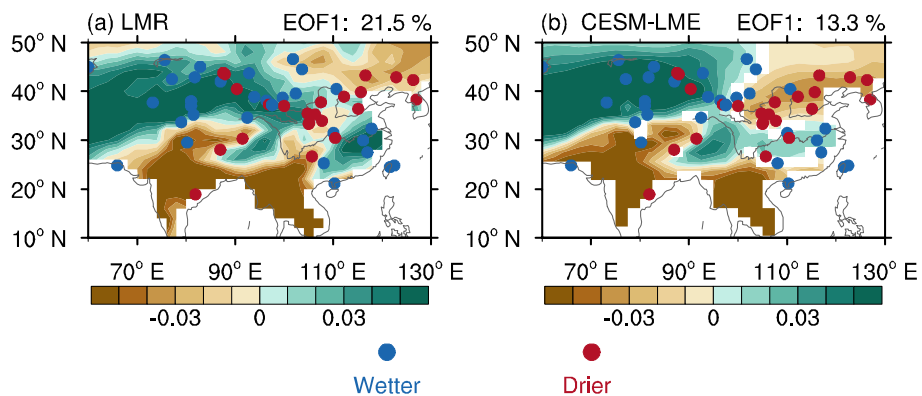
1 Introduction

The climate of the mid- to low-latitude Asian continent is characterized by an arid central Asian region and a moist monsoonal region. The climate in central Asia is mainly controlled by westerlies as a result of its geographical location and blocking by plateaus and mountains to the southeast (Chen et al., 2010). The main rainy seasons are spring and winter, especially in southern central Asia (Aizen et al., 2001; Chen et al., 2011; Xu et al., 2020; Wang et al., 2022). By contrast, the climate in monsoonal Asia is mainly controlled by the East Asian monsoon and the South Asian monsoon. The main rainy season is summer as a result of the warm, moist East Asian summer monsoon (Ding and Chan, 2005) and the South Asian summer monsoon (Turner and Annamalai, 2012).

The Asian arid and monsoonal climates should be independent of each other due to the dominance of different systems. However, the reconstruction records suggest a strong linkage between them on a centennial scale. Chen et al. (2015) reviewed numerous reconstruction studies and indicated that the climate was relatively wetter in central Asia and southern China, whereas it was relatively drier in northern China during the Little Ice Age (LIA; 1400–1900 AD) (Fig. 1). During the earlier Medieval Climate Anomaly (MCA; 1000–1300 AD), the wet and dry changes were the opposite, with drier conditions in central Asia and southern China and wetter conditions in northern China.

65
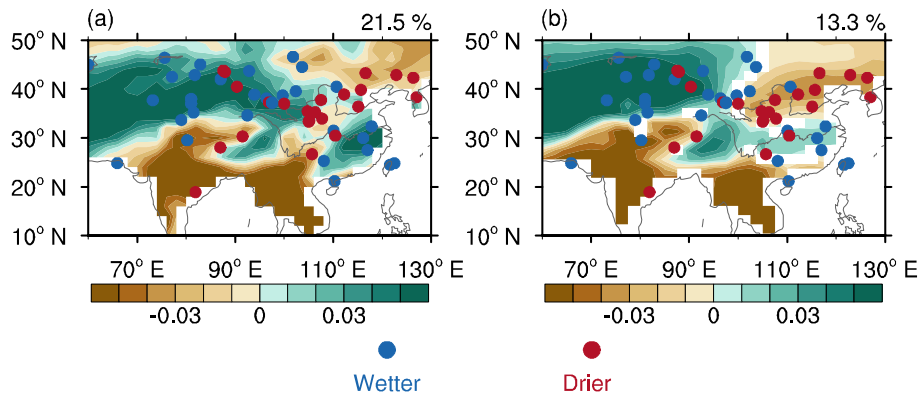
Figure 1. The reconstructed and simulated first leading precipitation mode. **(a)** The first leading mode (EOF1) of the nine-year low-pass Lanczos filtered annual precipitation for the time period 850–2000 in the Last Millennium Reanalysis (LMR) dataset. The explained variance is given at the top-right. **(b)** The average EOF1 of the nine-year low-pass Lanczos filtered annual precipitation in CESM-LME 12 all-forcing simulations for the time period 850–2005; the shading shows where at least two-thirds of the members agree on the sign of the average value. The averaged explained variance is given at the top-right. The dots represent the reconstructed precipitation/moisture records modified from Chen et al. (2015); the blue (red) dots denote wetter (drier) conditions in the LIA than in the MCA.

Clues to the linkage between the climate of the Asian arid regions and the Asian monsoon regions can also be found based on the limited length of observational data from the modern era. Since the mid-20th century, the central Asia has become wetter (Shi et al., 2007; Jiang et al., 2009; Chen et al., 2011; Huang et al., 2013). During the same period, southern China experienced more precipitation, whereas northern China received less precipitation and became drier (Ding et al., 2008; Zhao et al., 2010; Wang et al., 2013). Focusing on two different climatic regions, the precipitation observations during the period of 1960-2010 also show similar linkage (Huang et al., 2015). On a decadal scale, central Asia experienced more (less) summer precipitation, southern China received more (less) summer precipitation, whereas northern China

85   received less (more) summer precipitation.

86   However, the reconstruction records of the last millennium and the 50-year

87   observational data only cover less than two periods on the multi-centennial or

88   interdecadal scale, respectively. It is not sufficient to demonstrate a significant

89   relationship between the climate of the Asian arid regions and the Asian monsoon

90   regions. The specific mechanisms behind this possible linkage are still not clear. In

91   addition, modeling results also indicate that only one out of nine coupled models

92   within the Paleoclimate Modeling Intercomparison Project Phase 3 (PMIP3) is able to

93   reproduce the similar climatic linkage between the Asian arid and monsoonal regions

94   during the MCA and LIA (Shi et al., 2016). Due to the limitations of data length on

95   the time scales of interest and the large uncertainty in existing model results, therefore,

96   further research is still needed to confirm whether there is an inherent connection

97   between the arid regions and monsoon regions in Asia in terms of their dry-wet

98   variations.

99   In this study, we first focus on the decadal scale and intend to analyze whether

100   there is a robust linkage between the changes in precipitation pattern in arid regions

101   and monsoon regions in Asia using the newly released Last Millennium Reanalysis

102   (LMR) dataset (Tardif et al., 2019; Anderson et al., 2019). Additionally, to further

103   explore the possible mechanisms underlying the linkage and the potential impacts of

104   different external forcing factors, the Community Earth System Model Last

105   Millennium Ensemble (CESM-LME, Otto-Bliesner et al., 2016) is also utilized

106   because of its good performance in simulating Asian precipitation and summer

107 monsoon (e.g., Hu et al., 2023; Mishra and Aadhar, 2021; Shi et al., 2018) and the

108 availability of multiple samples forced by different forcing factors. Thus, the aim of

109 this study is to investigate the linkage between precipitation/moisture changes in arid

110 central Asia and monsoonal Asia during the last millennium and its driving factors.

111 The data and methods used in this study are described in detail in Sect. 2. The linkage

112 between the changes in precipitation/moisture pattern in arid regions and monsoon

113 regions in Asia is examined and its driving factors are analyzed in Sect. 3. Finally, the

114 discussion and conclusions are presented in Sect. 4 and Sect. 5, respectively.

115 **2 Data and methods**

116 **2.1 Reanalysis data and simulations**

117 In this study, we used the reconstructed annual precipitation anomalies (relative

118 to the climatological mean of 1951–1980) at a spatial resolution of 2° for the time

119 period 850–2000 from the LMR Version 2.1 dataset (Tardif et al., 2019; Anderson et

120 al., 2019) to examine the possible linkage between the Asian arid and monsoonal

121 regions. The proxy records assimilated in the LMR Version 2.1 dataset are from

122 PAGES-2k (PAGES2k, 2017). The analyses based on LMR were started with the

123 "grand mean", which was an average of 20 LMR reconstructions contained in

124 aforementioned array. In addition, the reconstructed sea surface temperature (SST)

125 anomalies from the LMR Version 2.1 dataset are also used to verify the model results.

126 In order to investigate the underlying mechanisms, we analyzed the monthly

127 outputs of CESM-LME project (Otto-Bliesner et al., 2016). The CESM-LME

128 simulations are performed using the CESM 1.1 model, in which the atmospheric

129   component is the Community Atmosphere Model Version 5 (CAM5) (Hurrell et al.,

130   2013). The atmosphere and land (ocean and sea ice) components in the CESM-LME

131   simulations have the same ~2° (~1°) horizontal resolutions as the CESM1.1 model.

132   We analyzed a total of 35 CESM-LME simulations: one control simulation, 12

133   all-forcing simulations and 22 single-forcing simulations. The single-forcing

134   simulations included a subset of five simulations forced by volcanic eruptions, a

135   subset of four simulations forced by solar activity, a subset of four simulations forced

136   by ozone and aerosols, three subsets of three simulations forced by greenhouse gases,

137   land use and land cover, and the Earth's orbit, respectively. The subset of simulations

138   forced by ozone and aerosols covered the time period 1850–2005, whereas the other

139   simulations were available for the time period 850–2005. The analyses for the

140   all-forcing simulations and the six subsets of single-forcing simulations were all based

141   on the arithmetic mean of multiple members, which was the final step in the analyses.

142   In addition, we also referred to reconstructed moisture/precipitation changes

143   (relative to the median of entire last millennium) in the LIA and MCA summarized by

144   Chen et al. (2015). The reconstructions synthesized by Chen et al. (2015) include 71

145   moisture/precipitation records derived from different types of proxy records (i.e., lake

146   record, speleothem record, historical documents, tree-ring record, ice-core record,

147   marine record, peat record, aeolian record, and river terrace). Based on these

148   moisture/precipitation records, figure 3 in Chen et al. (2015) provided the wetness

149   grades (i.e., the wetness was classified into dry, moderately dry, moderate, moderately

150   wet, and wet) for the LIA and MCA at individual sites. The 55 moisture/precipitation

151 records with different wetness grades between the LIA and MCA were selected in this

152 study to explore the moisture/precipitation changes between these two periods.

153 **2.2 Methods**

154 Following Henley et al. (2015), we defined the Interdecadal Pacific Oscillation

155 (IPO) index as the difference between the SST anomalies averaged over the

156 central-eastern equatorial Pacific (10 °S–10 °N, 170 °E–90 °W) and the average of the

157 SST anomalies over the western-central subtropical North Pacific (25–45 °N, 140 °E–

158 145 °W) and the western-central subtropical South Pacific (50–15 °S, 150 °E–160 °

159 W). The base period for calculating the IPO index was 1850–1900. To obtain the

160 filtered version of the index, a nine-year low-pass Lanczos filter was used, coinciding

161 with the other analyses in this study.

162 We used the aridity index (AI) to quantify the moisture condition of the

163 terrestrial climate (Middleton and Thomas, 1997):

164 $$AI = \frac{P}{PET} \tag{1}$$

165 where P is the annual precipitation (units: mm day^{-1}), representing the water supply to

166 land and PET is the annual potential evapotranspiration (units: mm day^{-1}), which

167 measures the atmospheric demand of water. A larger aridity index indicates that

168 relatively more moisture remains in the land, whereas a smaller aridity index

169 represents drier condition. The outputs of the CESM-LME simulations for soil

170 moisture (top 10 cm of soil; units: kg m^{-2}) were also analyzed to examine the analyses

171 based on the aridity index. Thus, the analyses related to moisture conditions in this

172 study were based on both the aridity index and soil moisture content.

173   The Penman–Monteith algorithm (Penman, 1948; Monteith, 1965) is widely

174   used to estimate the potential evapotranspiration and is recommended as a standard

175   method by the Food and Agriculture Organization of the United Nations (Allen et al.,

176   1998):

177    $$PET = \frac{0.408\Delta(R_n-G)+\gamma\frac{900}{T_{mean}+273}U(e_s-e_a)}{\Delta+\gamma(1+0.34U)} \qquad (2)$$

178   where the R_n is the net surface radiation (units: MJ m^{-2} day^{-1}), the G is soil heat flux

179   density (units: MJ m^{-2} day^{-1}); the difference between them represents the available

180   energy. γ is the psychrometric constant (units: kPa ℃$^{-1}$), T_{mean} is the mean

181   temperature (units: ℃; i.e., the average of the 2-m daily maximum and daily

182   minimum air temperatures); Δ is the slope vapor pressure curve (units: kPa ℃$^{-1}$)

183   derived from T_{mean}, U is the 2-m wind speed (units: m s^{-1}); e_s is the saturation vapor

184   pressure (units: kPa), derived from the daily maximum and daily minimum air

185   temperatures; e_a is the actual vapor pressure (units: kPa), calculated from e_s and the

186   relative humidity.

187   Empirical orthogonal function (EOF) analysis was performed on the

188   standardized annual precipitation to identify the first leading precipitation mode over

189   the Asian continent. A nine-year low-pass Lanczos filter was applied to the

190   standardized precipitation before EOF analysis to remove the variability on

191   interannual and shorter timescales. The same analyses were also applied to the aridity

192   index and the annual soil moisture content to obtain the first leading decadal moisture

193   mode over the Asian continent. Linear regression and correlation analyses were

194   applied to understand the root cause of the leading decadal precipitation/moisture

195 modes and their statistical significance was examined by a two-sided *t*-test. Because

196 of the low-pass Lanczos filter before linear regression and correlation analyses, the

197 effective degree of freedom N^* in the *t*-test was calculated following Bretherton et al.

198 (1999):

199 $$N^* = N \frac{1-r_a r_b}{1+r_a r_b} \qquad\qquad (3)$$

200 where r_a (r_b) is the autocorrelation at lag 1 for variables *a* (*b*) and *N* is the original

201 length of the time series. A two-sided *t*-test was also applied to examine the statistical

202 significance of climate changes between the LIA and the MCA. Besides, the

203 consistency of results derived from multiple members (i.e., analyses based on

204 all-forcing simulations and the six subsets of single-forcing simulations) was

205 examined by counting the percentage of members whose results' signs are the same as

206 the arithmetic mean of multiple members. A power spectrum analysis was performed

207 on the time series of the leading precipitation mode and the IPO index to obtain their

208 dominant periodicity, the statistical significance of which was examined via the power

209 spectrum of the mean red noise (Gilman et al., 1963).

210   In this study, winter, spring, summer, and autumn were defined as December–

211 February, March–May, June–August, and September–November, respectively.

212 **3 Results**

213 **3.1 Reconstructed and simulated first leading precipitation mode**

214   Based on the LMR data, the first leading mode (EOF1) of the decadal changes in

215 Asian precipitation in the last millennium showed the same changes in precipitation in

216 arid central Asia and southern China, which were the opposite of those in the South

217 Asian monsoon region (including the southern Tibetan Plateau, the Indian Peninsula

218 and the Indo-China Peninsula) and most of northern China (Fig. 1a). This mode

219 accounted for 21.5% of the total variance of precipitation in Asia in the last

220 millennium.

221 We also analyzed the outputs of the CESM-LME simulations. In the all-forcing

222 simulations, most members reproduced similar first leading precipitation mode with

223 the reconstruction for the time period 850–2005 (Fig. S1). Their ensemble pattern was

224 also consistent with the reconstruction (Fig. 1b). The averaged explained variance was

225 13.3% (ranging from 11.7 to 14.8%). These same patterns of changes in precipitation

226 between the long-term simulations and the reconstruction suggest that, on the decadal

227 scale, there is a robust linkage between the changes in precipitation pattern in arid

228 regions and monsoon regions. This decadal linkage suggests that the evolution of

229 precipitation in central Asia is out-of-phase with that in northern China and South

230 Asian monsoon region, but in-phase with that in southern China. The linkage between

231 the arid central Asian region and the East Asian monsoon region is consistent with the

232 relationship of changes in precipitation based on observational data for the last 60

233 years (Huang et al., 2015). Our analysis suggests that this observed relationship has

234 persisted over the last millennium. Our results also indicated that the decadal changes

235 in precipitation in the South Asian monsoon region are also closely related to the

236 changes in the arid central Asian region and the East Asian monsoon region.

237 **3.2 Dominant role of the IPO**

238 Many studies have shown that the SST anomaly is an important factor in

239   modulating the decadal variability in precipitation over Asia (e.g., Chu et al., 2018;

240   Huang et al., 2019). We therefore calculated the linear regression of the SST onto the

241   time series of the leading precipitation mode. Figure 2a and 2c show that higher

242   (lower) SSTs appeared over the central-eastern equatorial Pacific (the western-central

243   parts of both the subtropical North Pacific and South Pacific) in the LMR and

244   all-forcing simulations. The Pacific basin-wide SST anomalies resembled the positive

245   pattern of the IPO (Power et al., 1999; Henley et al., 2015; Wang and Miao, 2018).

246   The precipitation anomalies during the positive phases of the IPO showed positive

247   anomalies in arid central Asia and southern China and negative anomalies in the

248   South Asian monsoon region and most of northern China (Fig. 2b and 2d), resembling

249   the leading decadal precipitation mode in the LMR and all-forcing simulations. It is

250   therefore likely that the IPO dominated the decadal linkage between the changes in

251   precipitation pattern in arid regions and monsoon regions in Asia.
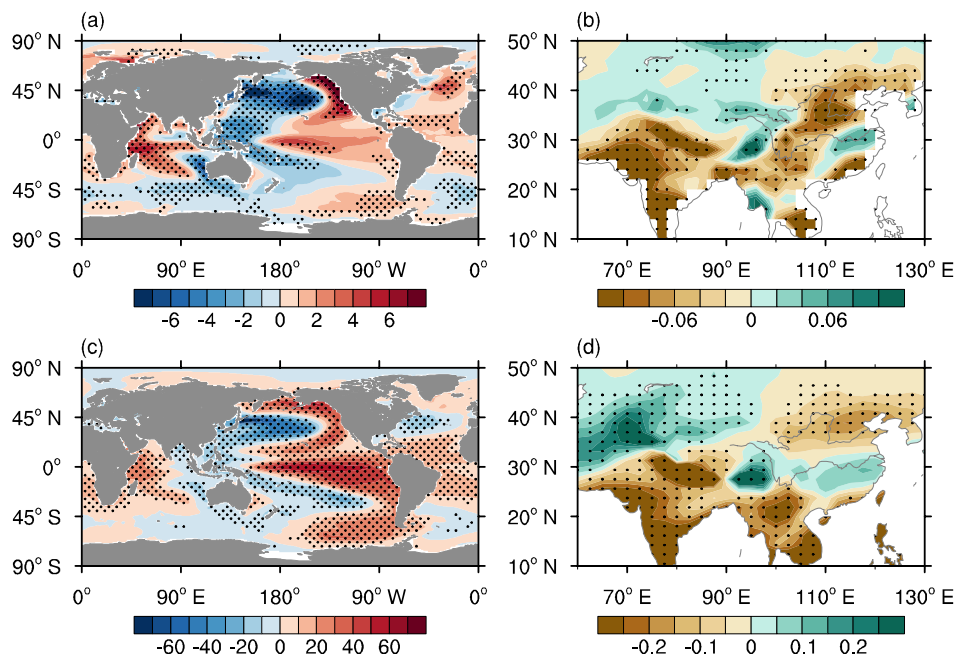
252

253   **Figure 2.** The dominant role of the IPO. The reconstructed **(a)** annual SST anomalies (units: °C)

254   regressed onto the time series of the leading decadal precipitation mode and **(b)** annual

255   precipitation anomalies (units: mm day^{-1}) regressed onto the time series of the IPO index in the

256   LMR dataset. The dots in parts (**a**, **b**) show significant anomalies at the 95% confidence level. (**c**)

257   Annual SST anomalies (units: °C) regressed onto time series of the leading decadal precipitation

258   mode and (**d**) annual precipitation anomalies (units: mm day^{-1}) regressed onto the time series of

259   the IPO index simulated by multiple members of the CESM-LME all-forcing runs. Dots in parts (**c**,

260   **d**) show that at least two-thirds of the members simulate significant changes (at the 95%

261   significance level), and these significant changes agree on the sign of the average of multiple

262   members.

263   We applied power spectrum analysis to explore the temporal characteristics of

264   the first leading precipitation mode and the IPO. Both the leading precipitation mode

265   and the IPO had a common frequency band of 10–20 years in the LMR and

266   all-forcing simulations (Figs. S2–4), indicating that the IPO dominated the linkage

267   between the changes in precipitation pattern in arid regions and monsoon regions in

268   Asia at decadal to bi-decadal scales during the last millennium. The consistency

269   between the reconstruction and the simulations indicates the reliability of the

270   simulations, which is the foundation of the following analyses on the relevant

271   mechanism based on simulations.

272   **3.3 Processes of the IPO modulating the leading precipitation pattern**

273   Because there is a seasonal cycle in precipitation and the atmospheric circulation

274   over Asia, especially over monsoonal Asia, we analyzed the seasonal changes in

275   precipitation associated with the IPO. During the positive phases of IPO, in the arid

276   central Asia, the precipitation in the four seasons all increased and made a positive

277   contribution to the increase in annual precipitation (Fig. 3). The precipitation

278   anomalies were larger in spring and winter, especially in spring, in which season the

279   precipitation accounted for the most of the annual precipitation (Fig. S5). The largest

280   increase in spring precipitation was mainly in southern central Asia. In East Asia,

281   summer precipitation increased (decreased) over southern (northern) China and

282   autumn precipitation decreased over northern China, both contributing positively to

283   the annual changes in precipitation. By contrast, spring and winter precipitation both

284   decreased over southern China, partly offsetting the positive contribution of summer

285   precipitation to the increase in annual precipitation in this region. Precipitation in all

286   four seasons decreased in most of the South Asian monsoon regions, contributing

287   positively to the decrease in annual precipitation. Then, we analyzed the seasonal

288   atmospheric circulation anomalies associated with the IPO to determine the processes

289   by which the IPO modulated these seasonal changes in precipitation.
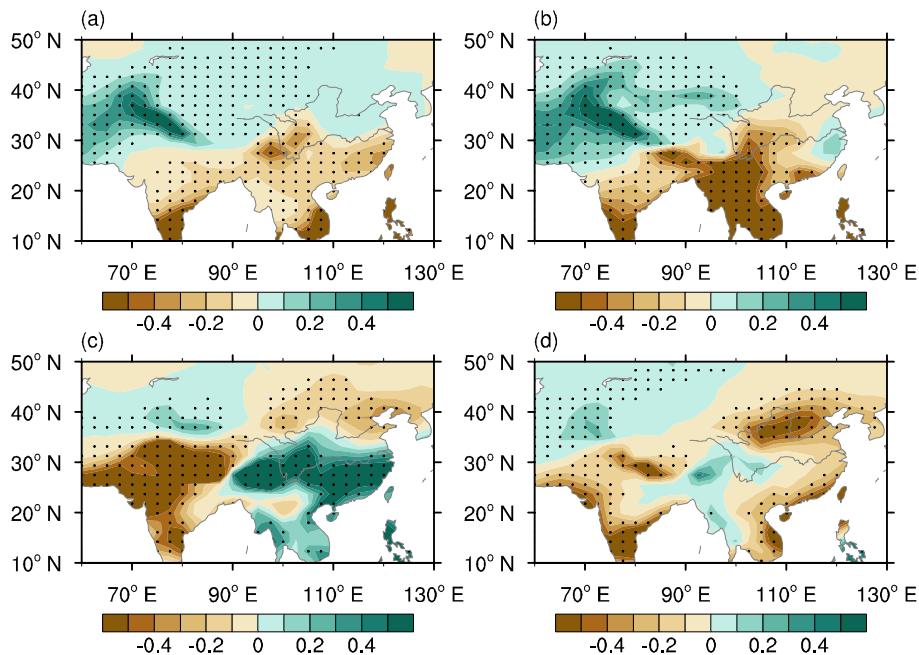
290

291   **Figure 3.** Simulated seasonal precipitation anomalies during the positive phases of the IPO.

292   Regressed maps of **(a)** winter, **(b)** spring, **(c)** summer, and **(d)** autumn precipitation anomalies

293   (units: mm day^{-1}) onto the time series of the IPO index simulated by multiple members of the

294   CESM-LME all-forcing runs. Dots show that at least two-thirds of the members simulate
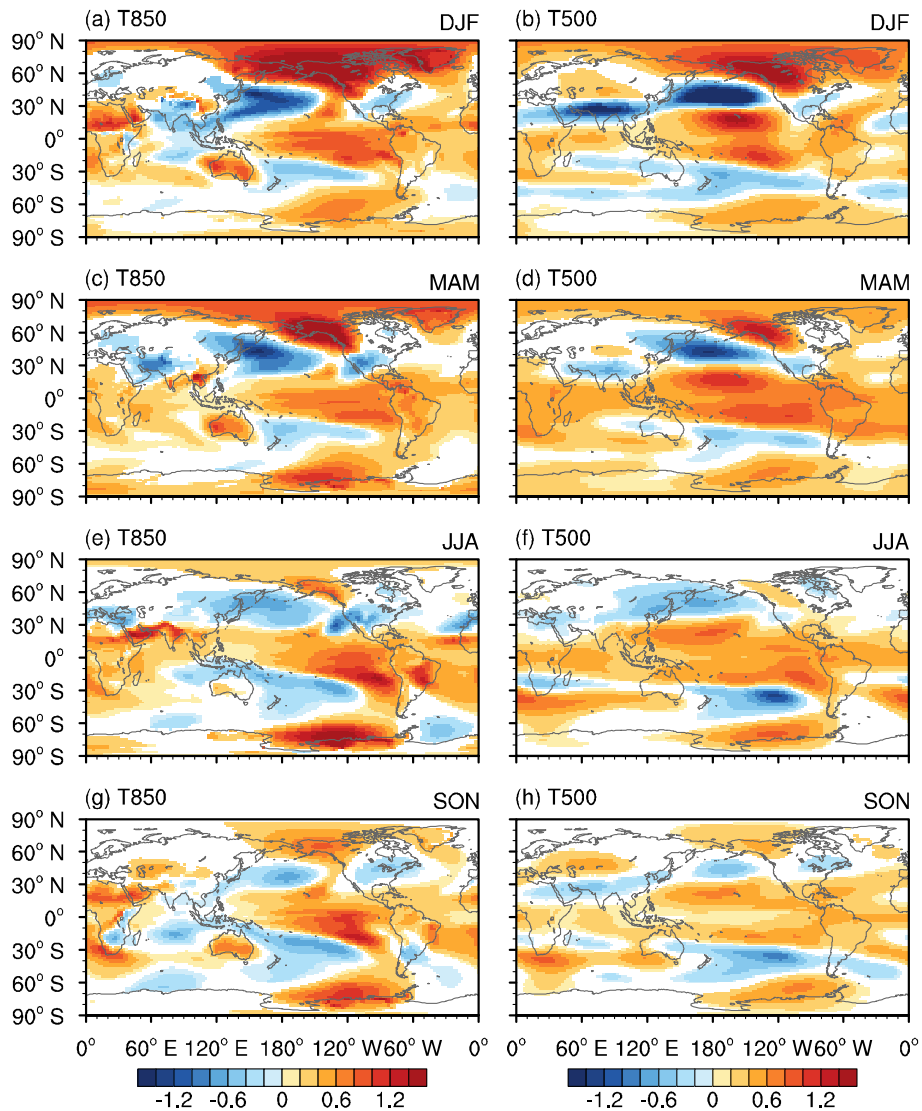
Figure 4. Simulated seasonal temperature anomalies during the positive phases of the IPO. Regressed maps of 850 hPa temperature anomalies (units: °C) in **(a)** winter, **(c)** spring, **(e)** summer, and **(g)** autumn onto the time series of the IPO index simulated by multiple members of the CESM-LME all-forcing runs. **(b)** Winter, **(d)** spring, **(f)** summer, and **(h)** autumn for 500 hPa temperature anomalies (units: °C). Shading shows that at least two-thirds of the members simulate significant changes (at the 95% significance level), and these significant changes agree on the sign of the average of multiple members.

3.3.1 Arid central Asia

306   In spring, warming appeared over the northern low and high latitudes, whereas

307   cooling appeared over the northern mid-latitudes, especially in the eastern hemisphere,

308   corresponding to a positive phase of the IPO (Fig. 4c and 4d). The tropospheric

309   temperature anomalies led to an enhanced (weakened) meridional temperature

310   gradient over low (high) latitudes as the climatological temperature decreased from

311   low to high latitudes. The anomalies in the temperature gradient contributed to

312   enhanced westerlies over low latitudes and weakened westerlies over high latitudes

313   via the thermal wind relation (Fig. 5c and 5d), indicating a southward shift of the

314   mid-latitude westerlies. The enhanced westerlies over the Mediterranean Sea and to

315   its east transported more water vapor from the Mediterranean Sea to southern central

316   Asia (Fig. 5a).

317   Positive sea-level pressure (SLP) anomalies appeared over the Indo–western

318   Pacific warm pool and negative SLP anomalies appeared over the eastern tropical

319   Pacific (Fig. 5c), consistent with the SST anomalies during positive IPO phases. The

320   distribution of the SLP anomalies indicated a weakened Walker circulation over the

321   Pacific Ocean, which further led to suppressed convection over the maritime continent

322   (Li et al., 2022). The decreased latent heating associated with the decreased

323   precipitation over the maritime continent can produce westward-propagating

324   baroclinic Rossby wave trains (Jiang et al., 2021). This resulted in anomalous

325   low-level anticyclone and upper-level cyclone over the Indian subcontinent, both of

326   which led to anomalous southerlies over central Asia (Fig. 5c and 5d). The anomalous

327   southerlies induced warm advection and led to anomalous ascending motion in this

328 region (Fig. 5b). In addition, the anomalous southerlies at low troposphere also could

329 transport more water vapor from low latitudes to central Asia (Fig. 5a). The enhanced

330 transport of water vapor and the anomalous ascending motion both favored increased

331 precipitation in spring over central Asia. In summary, the IPO affected the

332 precipitation from westerly winds through modulating the mid-latitude westerlies and

333 the Walker circulation in the Pacific Ocean.
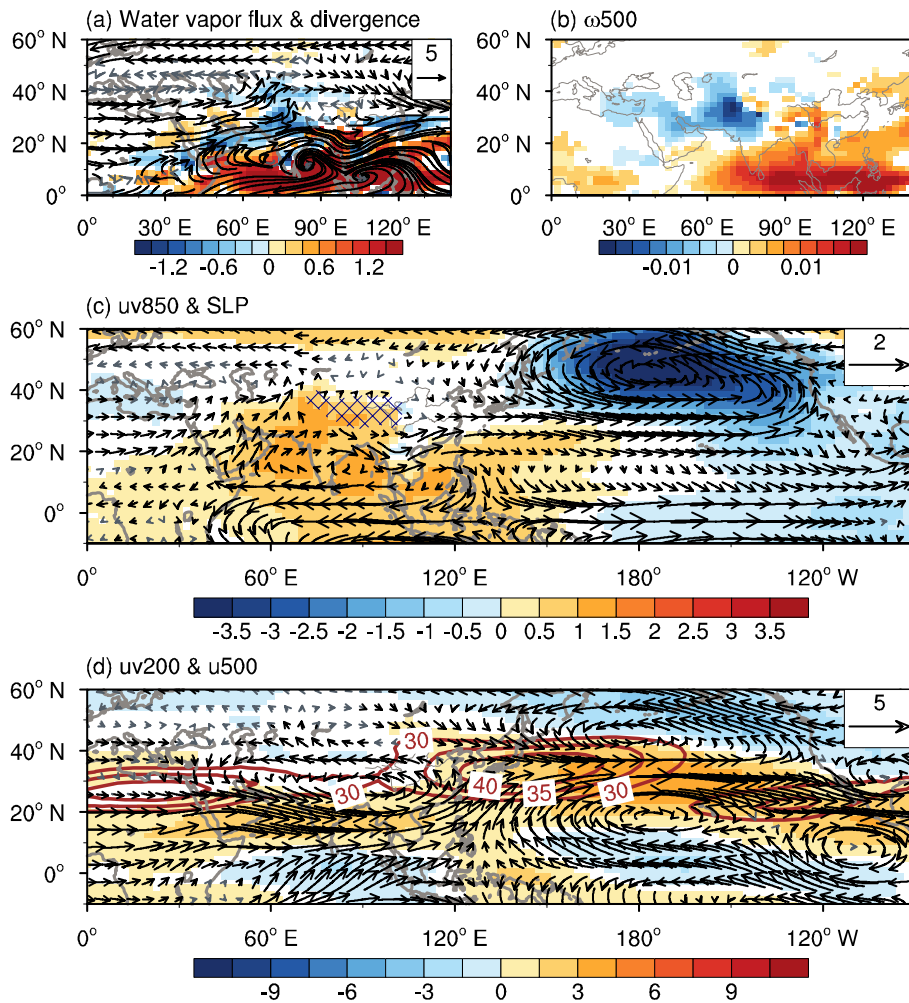
335 **Figure 5.** Simulated spring atmospheric circulation anomalies during the positive phases of the

336 IPO. Regressed maps of anomalous **(a)** vertically integrated water vapor flux from 1000 to 300

337 hPa (vectors; units: kg m^{-1} s^{-1}) and its divergence (shading; units: 10^{-5} kg m^{-2} s^{-1}), **(b)** 500 hPa

338 vertical velocity (ω500) (units: Pa s^{-1}), **(c)** 850 hPa wind (uv850) (vectors; units: m s^{-1}) and SLP

339 (shading; units: hPa), **(d)** 200 hPa wind (uv200) (vectors; units: m s^{-1}) and 500 hPa zonal wind

340 (u500) (shading; units: m s^{-1}) onto the time series of the IPO index simulated by the CESM-LME

341   all-forcing runs. The blue hatched patterns in part **(c)** indicate the region with an altitude >3000 m.

342   The brown contours in part **(d)** are the climatological 200 hPa zonal wind (units: m s^{-1}). The

343   shading shows that at least two-thirds of the members simulate significant changes (at the 95%

344   significance level), and these significant changes agree on the sign of the average of multiple

345   members. The black vectors show that for the zonal or meridional component, at least two-thirds

346   of the members simulate significant changes (at the 95% significance level), and these significant

347   changes agree on the sign of the average.

348   The circulation anomalies associated with the IPO in winter were similar to those

349   in spring (Fig. S6), indicating that the processes by which the IPO modulated winter

350   precipitation in central Asia were similar to those in spring.

351   **3.3.2 Asian monsoon regions**

352   In summer, higher (lower) SLPs appeared over the most of the Asian continent

353   (northern Pacific) during the positive phases of the IPO (Fig. 6c). This was the reverse

354   of the climatological state, in which the SLP over most of the Asian continent was

355   lower than that over the neighboring oceans. A weakened land–sea thermal contrast

356   was therefore induced. The weakened land–sea thermal contrast led to a weakened

357   Asian summer monsoon (ASM), featured by northerly anomalies at 850 hPa over the

358   whole of monsoonal Asia (Fig. 6c). The northerly anomalies further led to weakened

359   water vapor transport in this region (Fig. 6a).

360   Anomalies also appeared in the tropospheric temperature (Fig. 4e and 4f) and

361   caused westerly (easterly) anomalies over the south (north) of the climatological

362   Asian subtropical westerly jet at 200 hPa (Fig. 6d). The wind anomalies indicated the

363   southward shift in the Asian subtropical westerly jet and the associated secondary

364   meridional–vertical circulation (Cressman, 1981; Ding, 2005; Zhang and Huang,

2011), which led to anomalous downward motion over northern China and anomalous

upward motion over southern China (Fig. 6b) (Wang et al., 2013; Zhu et al., 2015).

The western Pacific subtropical high shifted southeastward (Fig. 6d), which did not

favor the transport of water vapor to northern China (Fig. 6a). These circulation

anomalies all indicate a weakened ASM system (Webster and Yang, 1992; Wang,

2001). Precipitation over southern China therefore increased in summer, whereas

precipitation over northern China and most of the South Asian monsoon regions

decreased. In summary, the IPO affected the monsoon precipitation through

modulating the ASM system.
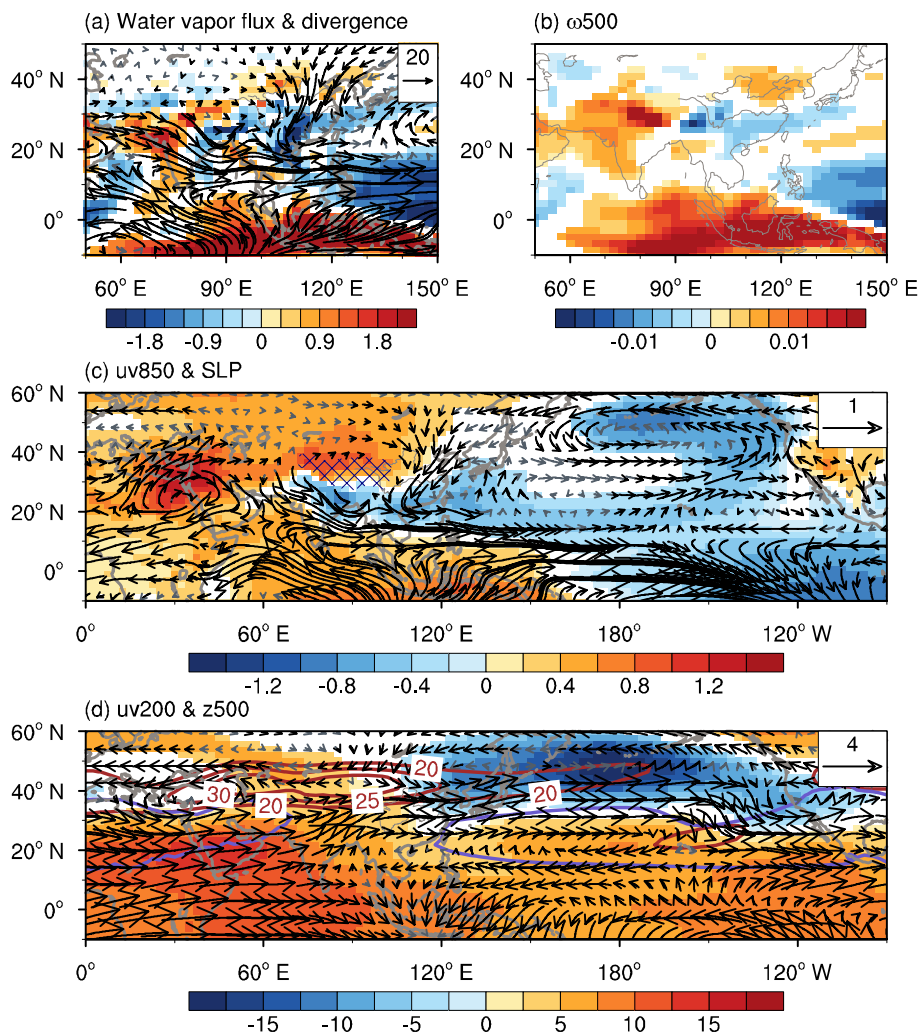
Figure 6. Simulated summer atmospheric circulation anomalies during the positive phases of the

IPO. Regressed maps of anomalous **(a)** vertically integrated water vapor flux from 1000 to 300 hPa (vectors; units: kg m^{-1} s^{-1}) and its divergence (shading; units: 10^{-5} kg m^{-2} s^{-1}), **(b)** 500 hPa vertical velocity (ω500) (units: Pa s^{-1}), **(c)** 850 hPa wind (uv850) (vectors; units: m s^{-1}) and SLP (shading; units: hPa), and **(d)** 200 hPa wind (uv200) (vectors; units: m s^{-1}) and 500 hPa geopotential height (z500) (shading; units: m) onto the time series of the IPO index simulated by the CESM-LME all-forcing runs. The blue hatched patterns in part **(c)** indicate the region with an altitude >3000 m. The brown contours in part **(d)** are the climatological 200 hPa zonal wind (units: m s^{-1}). The purple line in part **(d)** is the isoline with a value of 5860 m in the climatology state. The shading shows that at least two-thirds of the members simulate significant changes (at the 95% significance level), and these significant changes agree on the sign of the average of multiple members. The black vectors show that for the zonal or meridional component, at least two-thirds of the members simulate significant changes (at the 95% significance level), and these significant changes agree on the sign of the average.

In autumn, negative anomalies in the 500 hPa geopotential height appeared over the Korean Peninsula (Fig. S7d), indicating a strengthened East Asian trough (EAT) during the positive phases of the IPO (Qin et al., 2018, 2020; Li et al., 2020). The strengthened EAT contributed to northerly anomalies over East Asia (Fig. S7c), which led to weakened water vapor transport in this region (Fig. S7a). The anomalous northerlies to the west of the strengthened EAT induced cold advection (Fig. S7c and S7d) and led to anomalous descending motion over northern China (Fig. S7b). Precipitation therefore decreased over northern China in autumn.

Consistent with the SST anomalies during the positive phases of the IPO, positive (negative) SLP anomalies appeared over the Indo–western Pacific warm pool (eastern tropical Pacific) in all four seasons (Figs. 5c, 6c, S6c and S7c), indicating a weakened Walker circulation in the Pacific Ocean, which is in agreement with the

401 results in Dong and Lu (2013) and Zhao et al. (2021). This weakened Walker

402 circulation contributed to decreased precipitation over most of the South Asian

403 monsoon regions (Krishnamurthy and Krishnamurthy, 2014; Li et al., 2021).

3.4 Decisive role of internal variability

405 Many studies have suggested that both external forcings and internal variability

406 could affect the decadal variability of precipitation over Asia (e.g., Wang et al., 2013;

407 Jin et al., 2019; Zhu et al., 2022). To identify the roles of internal variability and

408 external forcing, Fig. 7 shows the first leading decadal precipitation modes of the

409 control and single-forcing simulations. The decadal linkage between the changes in

410 precipitation pattern in central Asia and monsoonal Asia in the all-forcing simulations

411 also appeared in the control simulation (Fig. 7a), implying this decadal linkage was

412 mainly caused by the internal variability. Nearly all the single-forcing simulations

413 presented similar decadal linkage with all-forcing simulations, apart from the

414 simulations forced by ozone and aerosols (Fig. 7b–g). This indicated that, during the

415 last millennium, volcanic eruptions, solar activity, greenhouse gases, land use and

416 land cover, and the Earth's orbit were unable to change the decadal linkage between

417 the changes in precipitation pattern in arid regions and monsoon regions in Asia,

418 which was dominated by the internal variability. Only in the ozone and aerosols

419 forcing simulations, which covered the period of 1850–2005, the decadal linkage of

420 precipitation changes disappeared. We further examined the results of other forcing

421 simulations for the period of 1850–2005 (Fig. S8), and all the first decadal

422 precipitation modes simulated by other forcing experiments still indicated similar

423   decadal linkage with all-forcing last-millennium simulations. This meant that since

424   the industrial revolution, only the ozone and aerosol forcing factors can change the

425   dominant mode of the reverse variation of precipitation in East Asia from north to

426   south and present stronger local climate effects. As noted by Wang et al. (2013), it

427   may be that anthropogenic aerosols play a more important role in regulating

428   precipitation in East Asia, which needs further analysis.
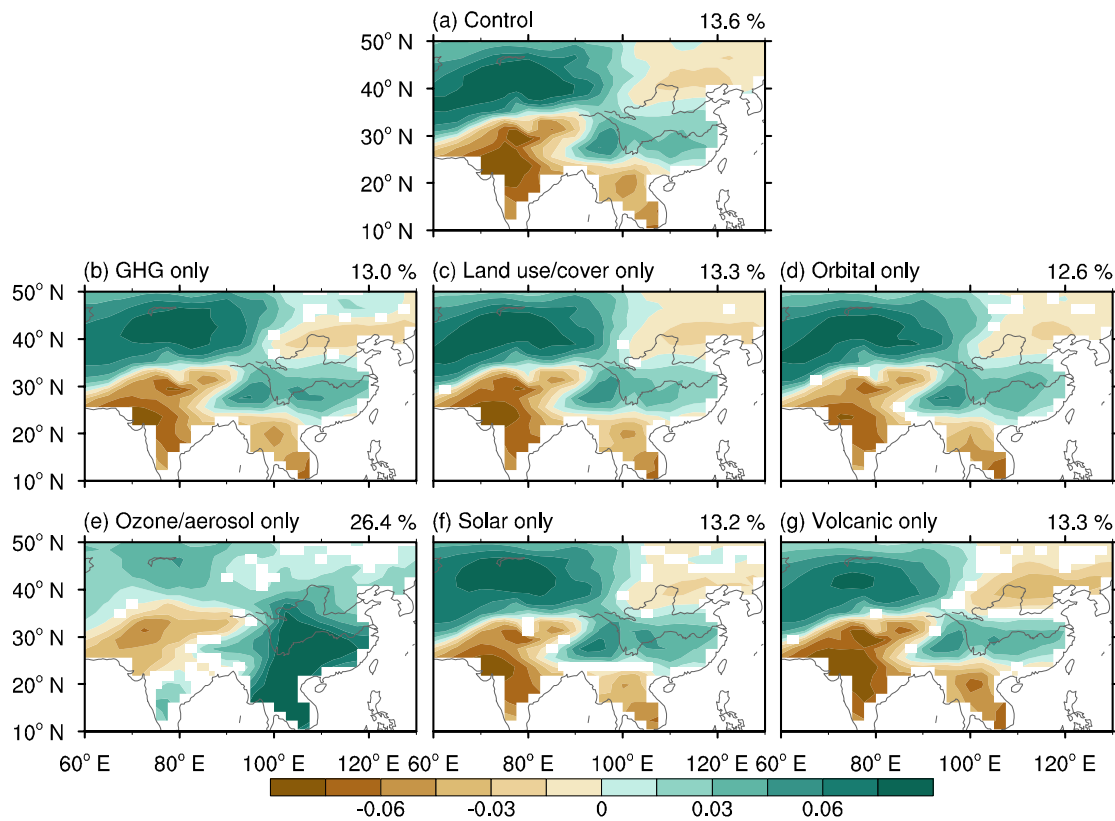
430   **Figure 7.** The leading decadal precipitation mode for the time period 850–2005 in the control and

431   single-forcing simulations, with the exception of leading mode for the time period 1850–2005 in

432   experiment forced by ozone and aerosols. **(a)** EOF1 of the nine-year low-pass Lanczos filtered

433   annual precipitation in the control simulation. The explained variance is given at the top-right. **(b–**

434   **g)** The average EOF1 of the nine-year low-pass Lanczos filtered annual precipitation in six subsets

435   of the single-forcing simulations: a subset of three simulations forced by greenhouse gas

436   emissions (GHG); a subset of three simulations forced by land use and land cover; a subset of

437   three simulations forced by the Earth's orbit; a subset of four simulations forced by ozone and

438   aerosols; a subset of four simulations forced by solar activity; and a subset of five simulations

439   forced by volcanic eruptions. The averaged explained variance is given at the top-right. The

440   shading in parts **(b–g)** shows where at least two-thirds of the members agree on the sign of the

441   average of multiple members.

442   Apart from the simulations forced by ozone and aerosols, the SST anomalies

443   associated with the leading precipitation mode in the control and single-forcing

444   simulations all showed a positive IPO pattern (Fig. S9), consistent with the all-forcing

445   simulations. At the same time, the precipitation anomalies associated with the positive

446   IPO in the control and single-forcing simulations all showed positive anomalies in

447   arid central Asia and southern China and negative anomalies in the South Asian

448   monsoon region and most of northern China (Fig. 8), also consistent with the

449   all-forcing simulations. This suggested that these external forcing factors cannot

450   change the dominant influence of IPO on Asian decadal precipitation and lead to the

451   decadal linkage between the changes in precipitation pattern in arid regions and

452   monsoon regions in Asia during the last millennium. It is therefore clear that the

453   internal variability associated with the IPO had a decisive role in shaping the decadal

454   linkage of precipitation changes.
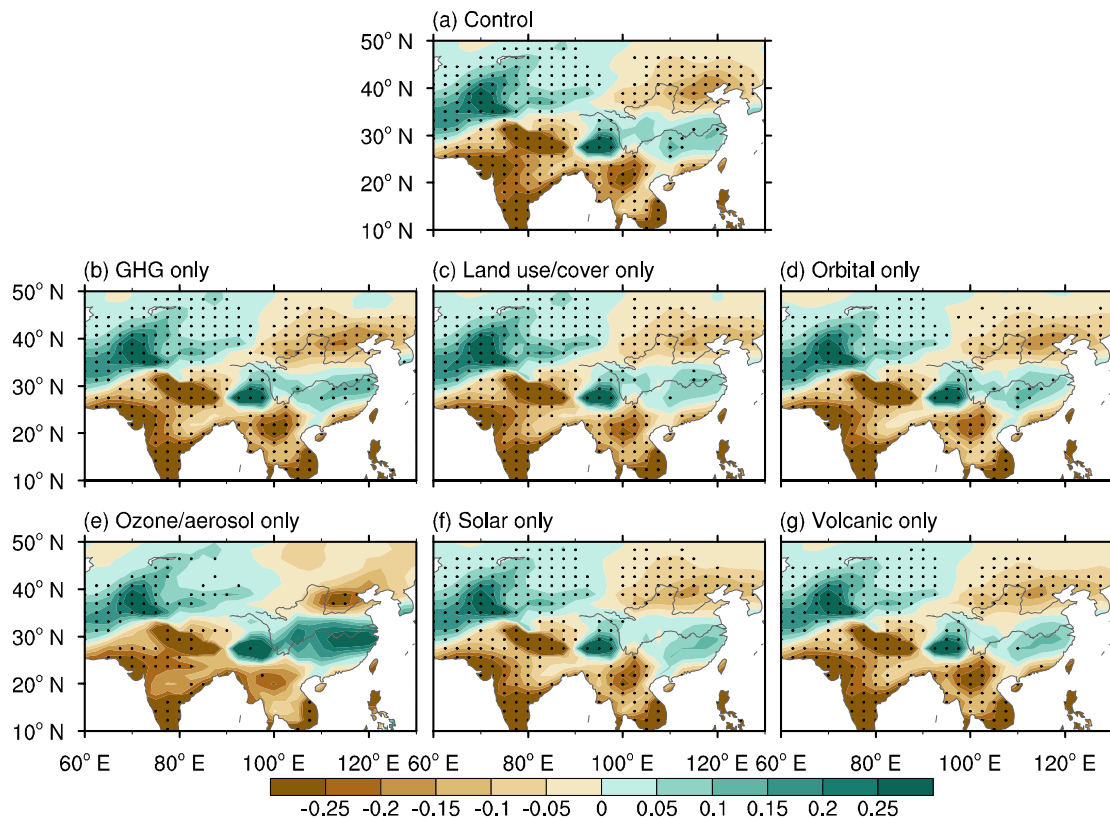
Figure 8. Simulated precipitation anomalies during the positive phases of the IPO in the control and single-forcing simulations. **(a)** Precipitation anomalies (units: mm day^{-1}) regressed onto the time series of the IPO index in the control run. **(b–g)** Precipitation anomalies (units: mm day^{-1}) regressed onto the time series of the IPO index in six subsets of the single-forcing simulations. The dots in part (a) show significant anomalies at the 95% confidence level and the dots in parts (b–g) denote that at least two-thirds of the members simulate significant changes (at the 95% significance level), and these significant changes agree on the sign of the average of multiple members.

In the ozone and aerosols forcing simulations, we can find positive precipitation anomalies in arid central Asia and southern China and negative precipitation anomalies in the South Asian monsoon region and most of northern China during the positive phases of the IPO (Fig. 8e). However, the changes in East Asian precipitation were no longer significant, which meant that the impacts of IPO on East Asian precipitation in this experiment were weakened.

3.5 Simulated first leading moisture mode

Terrestrial moisture conditions are closely related to precipitation changes and could strongly affect terrestrial ecosystems. The terrestrial moisture condition is quantified by both aridity index and soil moisture content here. Based on our analyses of the aridity index (Fig. 9a) and the soil moisture content (Fig. S10a), we found that the EOF1 of the decadal changes in Asian moisture during the last millennium also showed the same changes in moisture in arid central Asia and southern China, which were the opposite of those in the South Asian monsoon region and most of northern China. This is consistent with the first leading precipitation mode, suggesting the important contribution of precipitation to the decadal linkage between the changes in moisture pattern in arid regions and monsoon regions in Asia. Similar first leading moisture mode was seen in all the experiments apart from those with only ozone and aerosol forcing (Figs. 9 and S10), indicating the decisive role of internal variability on the decadal linkage of moisture changes.
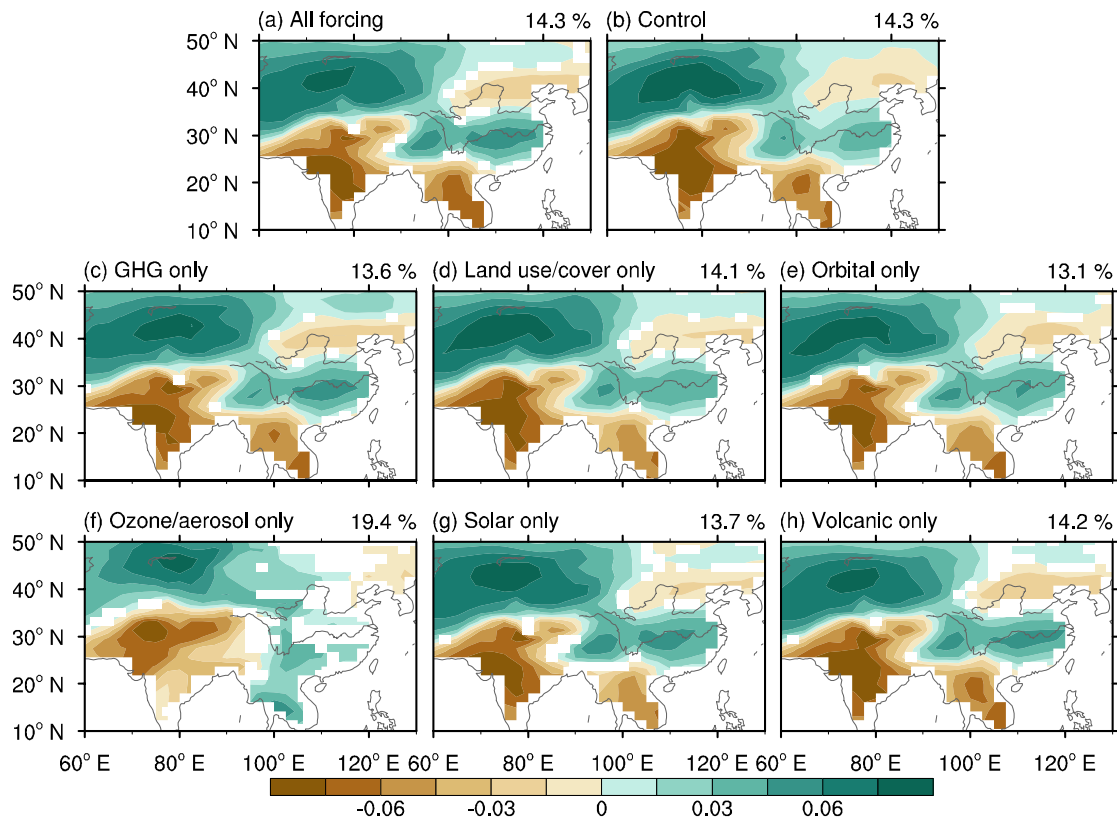
Figure 9. The simulated leading decadal aridity index mode for the time period 850–2005 in all the experiments, with the exception of leading mode for the time period 1850–2005 in experiment forced by ozone and aerosols. **(a)** The average EOF1 of the nine-year low-pass Lanczos filtered aridity index in the all-forcing simulations. The averaged explained variance is given at the top-right. **(b)** EOF1 of the nine-year low-pass Lanczos filtered aridity index in the control simulation. The explained variance is given at the top-right. **(c–h)** The average EOF1 of the nine-year low-pass Lanczos filtered aridity index in six subsets of the single-forcing simulations. The averaged explained variance is given at the top-right. The shading in parts **(a, c–h)** shows where at least two-thirds of the members agree on the sign of the average of multiple members.

The SST anomalies associated with the leading moisture mode in all experiments, apart from those with only ozone and aerosol forcing, showed a positive IPO pattern (Figs. S11 and S12), indicating the dominant role of the IPO on the decadal linkage of moisture changes. The moisture anomalies associated with the positive IPO showed positive anomalies in arid central Asia and southern China and negative anomalies in

499   the South Asian monsoon region and most of northern China in all the experiments

500   (Figs. 10 and S13), consistent with the leading moisture mode. This further confirmed

501   the aforementioned dominant role of the IPO. Therefore, the internal variability

502   associated with the IPO also had a decisive role in shaping the decadal linkage

503   between the changes in moisture pattern in arid regions and monsoon regions in Asia

504   through regulating precipitation during the last millennium.
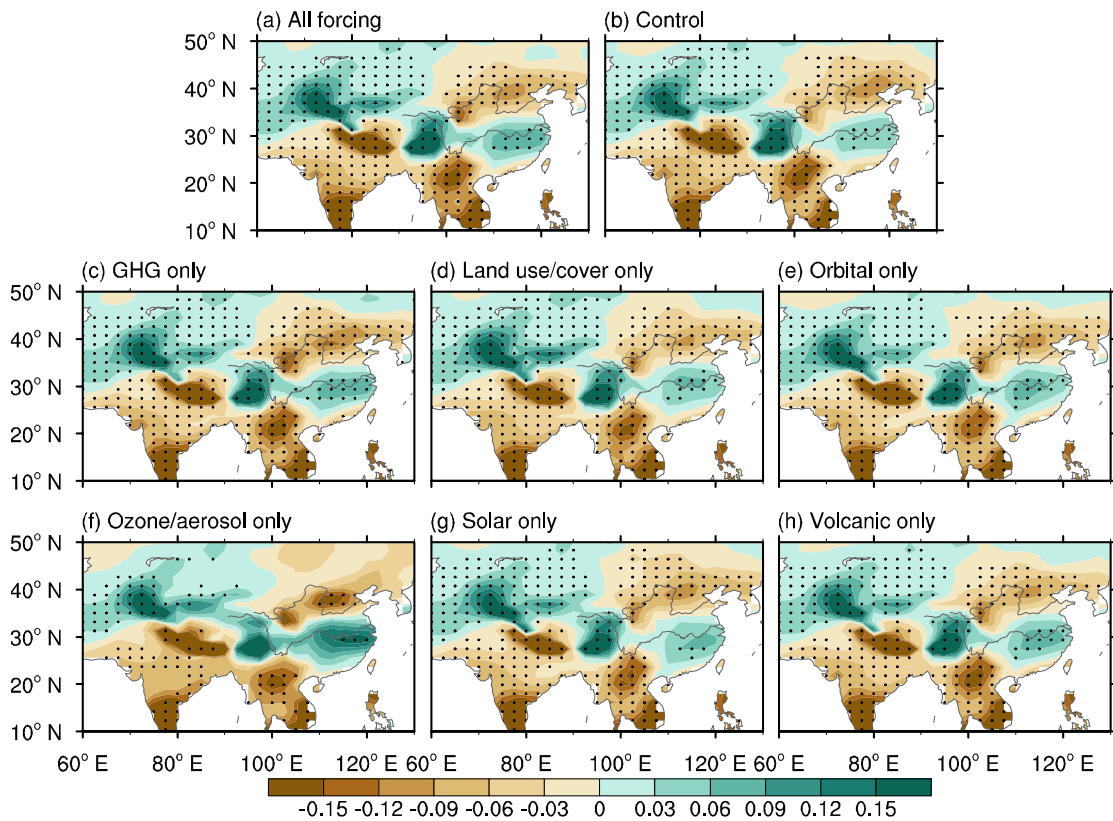
505

506   **Figure 10.** Simulated aridity index anomalies during the positive phases of the IPO. The aridity

507   index anomalies regressed onto the time series of the IPO index in the **(a)** all-forcing simulations,

508   **(b)** control simulation, and **(c–h)** six subsets of the single-forcing simulations. The dots in part **(b)**

509   show significant anomalies at the 95% confidence level and the dots in parts **(a, c–h)** denote that

510   at least two-thirds of the members simulate significant changes (at the 95% significance level),

511   and these significant changes agree on the sign of the average of multiple members.

512   **4 Discussion**

4.1 Limited impacts of external forcings on decadal precipitation linkage

As stated in section 3.4, the spatial pattern of leading decadal precipitation mode in all-forcing simulations also appears in control and all single-forcing simulations, apart from the simulations forced by ozone and aerosols. This indicates the dominant role of internal variability in shaping the spatial pattern of leading decadal precipitation mode during the last millennium. Moreover, this process can be partially influenced by the impacts of ozone and aerosol forcing since the industrial revolution. During this period, ozone and aerosols have played crucial roles in regulating the climate at mid-latitudes in the Northern Hemisphere (Miao et al., 2022). However, the relative impact of internal variability and external forcings on the time variations of the leading decadal precipitation mode during the last millennium remains unclear. Thus, we calculated the correlations across the time series of the leading decadal precipitation mode (i.e., the principal components) simulated by CESM-LME 12 all-forcing simulations (Table S1). Except for autocorrelations for each principal component, the other correlations range from -0.06 to 0.35, and only 13.6% correlations are significant at the 95% confidence level. These relatively small correlations indicate the impacts of external forcings on the time variations of the leading decadal precipitation mode are very weak. The several significant correlations suggest that, to a limited extent, the time variations of the leading decadal precipitation mode could be affected by external forcings (e.g., volcanic eruptions and solar radiation) (Ning et al., 2020; Xue et al., 2023). Therefore, internal variability played a dominant role in shaping the time variations of the leading decadal

535   precipitation mode.

536   In summary, the impacts of external forcings on both spatial pattern and time

537   variations of the leading decadal precipitation mode are relatively weak, which

538   indicates limited impacts of external forcings on decadal linkage between

539   precipitation changes in arid central Asia and humid monsoonal Asia during the last

540   millennium. This is quite different from the dominating role of external forcings in

541   regulating the variations of Asian precipitation at suborbital and longer timescales (Xu

542   et al., 2023).

543   **4.2 Centennial precipitation/moisture linkage**

544   The features of decadal linkage between moisture/precipitation changes in arid

545   central Asia and humid monsoonal Asia during the last millennium have been

546   investigated and the dynamic mechanisms associated with the decadal linkage have

547   been explored above. Next, the potential linkage on multi-centennial scale implied by

548   reconstruction is discussed here. Between the LIA and MCA, on multi-centennial

549   scale, wetter (drier) conditions over arid central Asia and southern China (most of

550   northern China) were reconstructed in Chen et al. (2015) (Fig. 11a). Besides, the

551   changes in precipitation between the LIA and the MCA based on the LMR showed

552   more (less) precipitation over eastern central Asia and southern China (the South

553   Asian monsoon region and most of northern China) (Fig. 11a), consistent with the

554   reconstructed changes in precipitation/moisture in Chen et al. (2015). These results

555   suggest a robust centennial linkage of the changes in precipitation/moisture in central

556   Asia and monsoonal Asia, similar to the decadal precipitation/moisture linkage.
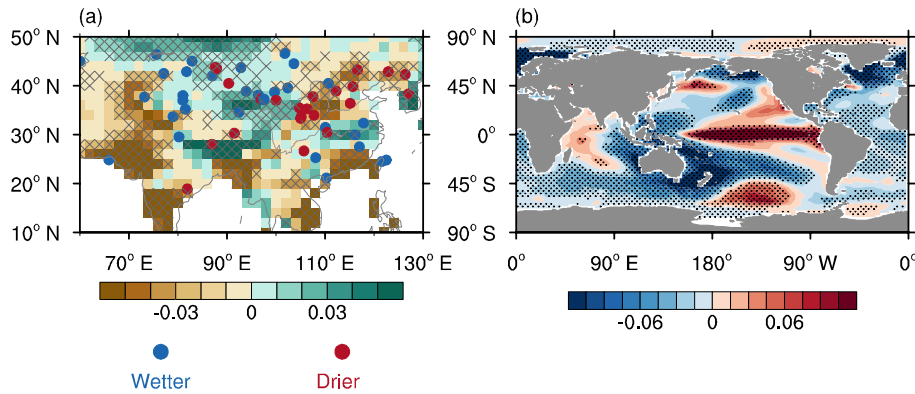
Figure 11. Reconstructed changes in **(a)** precipitation (units: mm day^{-1}) and **(b)** SST (units: °C) between the LIA and MCA in the LMR. The gray hatched patterns in part **(a)** and black dots in part **(b)** indicate significant anomalies at the 95% confidence level. The dots in part **(a)** represent the reconstructed precipitation/moisture records modified from Chen et al. (2015); the blue (red) dots denote wetter (drier) conditions in the LIA than in the MCA.

The reconstructed changes in the SST between the LIA and MCA showed higher (lower) SSTs over the central-eastern equatorial Pacific (the western-central parts of both the subtropical North Pacific and South Pacific) (Fig. 11b). According to the present study, the IPO-like condition may be the primary cause of the centennial linkage of changes in precipitation/moisture in central Asia and monsoonal Asia. However, most current models still cannot reproduce the evolution of the Pacific Decadal Oscillation (Wang and Miao, 2018). The CESM-LME simulations were also unable to produce the reconstructed centennial changes in SST between the LIA and MCA. Therefore, in the present study, we cannot directly obtain the evidence of the aforementioned centennial linkage from the CESM-LME results. The failure of CESM-LME simulations in reproducing the centennial linkage further limits our understanding of the relative roles of the external forcings and internal variability in shaping the centennial linkage. Thus, further investigation remains needed.

5 Conclusions

Based on the LMR dataset and CESM-LME all-forcing simulations, the first leading precipitation mode in Asia on decadal scale during the last millennium showed the same changes in precipitation in arid central Asia and southern China, which were the opposite of those in the South Asian monsoon region and most of northern China. This mode indicated a robust linkage between the changes in precipitation pattern in arid regions and monsoon regions in Asia on decadal scale, in which the evolution of precipitation in central Asia was out-of-phase with that of northern China and the South Asian monsoon regions and in-phase with that of southern China.

Further analysis based on CESM-LME all-forcing, control and all single-forcing simulations showed that the internal variability associated with the IPO plays a dominant role in connecting the decadal variations in precipitation between arid central Asia and monsoonal Asia by modulating the precipitation of their respective major rainy seasons during the last millennium. In spring, the positive IPO could enhance westerlies over the Mediterranean Sea and to its east, which could transport more water vapor and cause increased precipitation over central Asia. In summer, the positive IPO is accompanied with weakened Asian summer monsoon and southward Asian subtropical westerly jet, which further lead to increased (decreased) summer precipitation over southern China (over northern China and South Asian monsoon region). Besides, the positive IPO can weaken Pacific Walker circulation, which contributes to precipitation decrease over South Asian monsoon regions in all four

598   seasons.

599   In addition, this decadal linkage of precipitation variation also causes a similar

600   decadal linkage of moisture changes in central Asia and monsoonal Asia during the

601   last millennium.

602

603   **Data availability.** The Last Millennium Reanalysis (LMR) Version 2.1 dataset (Tardif

604   et al., 2019; Anderson et al., 2019) used in this study are available at

605   https://www.atmos.uw.edu/~hakim/LMR/. The Community Earth System Model-Last

606   Millennium Ensemble (CESM-LME) (Otto-Bliesner et al., 2016) can be founded at

607   https://www.cesm.ucar.edu/community-projects/lme.

608

609   **Author contributions**. TW designed the study; HX analyzed the dataset and plotted

610   the figures; HX, TW and HW all contributed to writing the manuscript and

611   interpreting results; Funding was acquired by TW and HX.

612

613   **Competing interests.** The authors declare that they have no conflict of interest.

614

615   **Acknowledgements.** We sincerely thank two anonymous reviewers and editor for

616   their valuable comments and suggestions, which helped to improve the quality of this

617   paper significantly. This research has been supported by the National Natural Science

618   Foundation of China (Grant No. 42221004), the National Key Research and

619   Development Program of China (Grant No. 2018YFA0606403), and the Postgraduate

620   Research and Practice Innovation Program of Jiangsu Province (KYCX21_0944).

621

622   **References**

623   Aizen, E. M., Aizen, V. B., Melack, J. M., Nakamura, T., and Ohta, T.: Precipitation

624   and atmospheric circulation patterns at mid-latitudes of Asia, Int. J. Climatol., 21,

625   535–556, https://doi.org/10.1002/joc.626, 2001.

626   Allen,   R.   G.,   Pereira,   L.   S.,   Raes,   D.,   and   Smith,   M.:   Crop

627   evapotranspiration-guidelines for computing crop water requirements, Food and

628   Agriculture Organization of the United Nations Irrigation and Drainage Paper 56,

629   1–326, 1998.

630   Anderson, D. M., Tardif, R., Horlick, K., Erb, M. P., Hakim, G. J., Noone, D., Perkins,

631   W. A., and Steig, E.: Additions to the Last Millennium Reanalysis multi-proxy

632   database, Data Science Journal, 18, 1–11, http://doi.org/10.5334/dsj-2019-002,

633   2019.

634   Bretherton, C. S., Widmann, M., Dymnikov, V. P., Wallace, J. M., and Bladé, I.: The

635   effective number of spatial degrees of freedom of a time-varying field, J. Climate,

636   12,   1990–2009,

637   https://doi.org/10.1175/1520-0442(1999)012<1990:tenosd>2.0.co;2, 1999.

638   Chen, F., Chen, J., Holmes, J., Boomer, I., Austin, P., Gates, J. B., Wang, N., Brooks,

639   S. J., and Zhang, J.: Moisture changes over the last millennium in arid central

640   Asia: a review, synthesis and comparison with monsoon region, Quaternary Sci.

641   Rev., 29, 1055–1068, https://doi.org/10.1016/j.quascirev.2010.01.005, 2010.

Chen, F., Huang, W., Jin, L., Chen, J., and Wang, J.: Spatiotemporal precipitation variations in the arid Central Asia in the context of global warming, Sci. China Earth Sci., 54, 1812–1821, https://doi.org/10.1007/s11430-011-4333-8, 2011.

Chen, J., Chen, F., Feng, S., Huang, W., Liu, J., and Zhou, A.: Hydroclimatic changes in China and surroundings during the Medieval Climate Anomaly and Little Ice Age: spatial patterns and possible mechanisms, Quaternary Sci. Rev., 107, 98–111, https://doi.org/10.1016/j.quascirev.2014.10.012, 2015.

Chu, C., Yang, X.-Q., Sun, X., Yang, D., Jiang, Y., Feng, T., and Liang, J.: Effect of the tropical Pacific and Indian Ocean warming since the late 1970s on wintertime Northern Hemispheric atmospheric circulation and East Asian climate interdecadal changes, Clim. Dynam., 50, 3031–3048, https://doi.org/10.1007/s00382-017-3790-y, 2018.

Cressman, G. P.: Circulations of the west Pacific jet stream, Mon. Weather Rev., 109, 2450–2463, https://doi.org/10.1175/1520-0493(1981)109<2450:cotwpj>2.0.co;2, 1981.

Ding, Y.: Advanced synoptic meteorology, China Meteorological Press, Beijing, 2005.

Ding, Y. and Chan, J. C. L.: The East Asian summer monsoon: an overview, Meteorol. Atmos. Phys., 89, 117–142, https://doi.org/10.1007/s00703-005-0125-z, 2005.

Ding, Y., Wang, Z., and Sun, Y.: Inter-decadal variation of the summer precipitation in East China and its association with decreasing Asian summer monsoon. Part I: Observed evidences, Int. J. Climatol., 28, 1139–1161, https://doi.org/10.1002/joc.1615, 2008.

Dong, B. and Lu, R.: Interdecadal enhancement of the walker circulation over the

Tropical Pacific in the late 1990s, Adv. Atmos. Sci., 30, 247–262,

https://doi.org/10.1007/s00376-012-2069-9, 2013.

Gilman, D. L., Fuglister, F. J., and Mitchell, J. M.: On the power spectrum of "red

noise",   J.   Atmos.   Sci.,   20,   182–184,

https://doi.org/10.1175/1520-0469(1963)020<0182:otpson>2.0.co;2, 1963.

Henley, B. J., Gergis, J., Karoly, D. J., Power, S., Kennedy, J., and Folland, C. K.: A

Tripole Index for the Interdecadal Pacific Oscillation, Clim. Dynam., 45, 3077–

3090, https://doi.org/10.1007/s00382-015-2525-1, 2015.

Hu, Y., Sun, W., Liu, J., Chen, D., Ning, L., and Peng, Z.: Decadal variability of

precipitation over the Tibetan Plateau modulated by the 11-year solar cycle over

the   past   millennium,   Front.   Earth   Sci.,   11,

https://doi.org/10.3389/feart.2023.1137205, 2023.

Huang, J., Ma, J., Guan, X., Li, Y., and He, Y.: Progress in semi-arid climate change

studies   in   China,   Adv.   Atmos.   Sci.,   36,   922–937,

https://doi.org/10.1007/s00376-018-8200-9, 2019.

Huang, W., Chen, F., Feng, S., Chen, J., and Zhang, X.: Interannual precipitation

variations in the mid-latitude Asia and their association with large-scale

atmospheric   circulation,   Chinese   Sci.   Bull.,   58,   3962–3968,

https://doi.org/10.1007/s11434-013-5970-4, 2013.

Huang, W., Chen, J., Zhang, X., Feng, S., and Chen, F.: Definition of the core zone of

the "westerlies-dominated climatic regime", and its controlling factors during the

686   instrumental period, Sci. China Earth Sci., 58, 676–684,

687   https://doi.org/10.1007/s11430-015-5057-y, 2015.

688   Hurrell, J. W., Holland, M. M., Gent, P. R., Ghan, S., Kay, J. E., Kushner, P. J.,

689   Lamarque, J.-F., Large, W. G., Lawrence, D., Lindsay, K., Lipscomb, W. H.,

690   Long, M. C., Mahowald, N., Marsh, D. R., Neale, R. B., Rasch, P., Vavrus, S.,

691   Vertenstein, M., Bader, D., Collins, W. D., Hack, J. J., Kiehl, J., and Marshall, S.:

692   The Community Earth System Model: A framework for collaborative research, B.

693   Am. Meteorol. Soc., 94, 1339–1360, https://doi.org/10.1175/bams-d-12-00121.1,

694   2013.

695   Jiang, D., Su, M., Wei, R., and Bao, L.: Variation and projection of drought and wet

696   conditions in Xinjiang, Chinese Journal of Atmospheric Sciences, 33, 90–98,

697   https://doi.org/10.3878/j.issn.1006-9895.2009.01.08, 2009.

698   Jiang, J., Zhou, T., Chen, X., and Wu, B.: Central Asian precipitation shaped by the

699   tropical Pacific Decadal Variability and the Atlantic Multidecadal Variability, J.

700   Climate, 34, 7541–7553, https://doi.org/10.1175/jcli-d-20-0905.1, 2021.

701   Jin, C., Liu, J., Wang, B., Yan, M., and Ning, L.: Decadal variations of the East Asian

702   summer monsoon forced by the 11-year insolation cycle, J. Climate, 32, 2735–

703   2745, https://doi.org/10.1175/jcli-d-18-0288.1, 2019.

704   Krishnamurthy, L. and Krishnamurthy, V.: Influence of PDO on South Asian summer

705   monsoon and monsoon–ENSO relation, Clim. Dynam., 42, 2397–2410,

706   https://doi.org/10.1007/s00382-013-1856-z, 2014.

707   Li, B., Li, Y., Chen, Y., Zhang, B., and Shi, X.: Recent fall Eurasian cooling linked to

North Pacific sea surface temperatures and a strengthening Siberian high, Nat. Commun., 11, 5202, https://doi.org/10.1038/s41467-020-19014-2, 2020.

Li, G., Gao, C., Lu, B., and Chen, H.: Inter-annual variability of spring precipitation over the Indo-China Peninsula and its asymmetric relationship with El Niño-Southern Oscillation, Clim. Dynam., 56, 2651–2665, https://doi.org/10.1007/s00382-020-05609-4, 2021.

Li, T., Wang, Y., Wang, B., Ting, M., Ding, Y., Sun, Y., He, C., and Yang, G.: Distinctive South and East Asian monsoon circulation responses to global warming, Sci. Bull., 67, 762–770, https://doi.org/10.1016/j.scib.2021.12.001, 2022.

Miao, J., Wang, T., and Jiang, D.: Ozone-aerosol and land use reversed temperature increase over some northern mid-latitude regions between the 20th century and the Little Ice Age based on the CESM-LME, The Holocene, 32, 1251–1259, https://doi.org/10.1177/09596836211041734, 2022.

Middleton, N. J. and Thomas, D. S. G.: World atlas of desertification, 2nd edn, Edward Arnold, London, The United Kingdom, 1997.

Mishra, V. and Aadhar, S.: Famines and likelihood of consecutive megadroughts in India, npj Clim. Atmos. Sci., 4, 59, https://doi.org/10.1038/s41612-021-00219-1, 2021.

Monteith, J. L.: Evaporation and environment, Symposia of the Society for Experimental Biology, 19, 205–234, 1965.

Ning, L., Chen, K., Liu, J., Liu, Z., Yan, M., Sun, W., Jin, C., and Shi, Z.: How do

volcanic eruptions influence decadal megadroughts over eastern China?, J. Climate, 33, 8195–8207, https://doi.org/10.1175/JCLI-D-19-0394.1, 2020.

Otto-Bliesner, B. L., Brady, E. C., Fasullo, J., Jahn, A., Landrum, L., Stevenson, S., Rosenbloom, N., Mai, A., and Strand, G.: Climate variability and change since 850 CE: An ensemble approach with the Community Earth System Model, B. Am. Meteorol. Soc., 97, 735–754, https://doi.org/10.1175/bams-d-14-00233.1, 2016.

PAGES2k Consortium: A global multiproxy database for temperature reconstructions of the Common Era, Sci. Data, 4, 170088, https://doi.org/10.1038/sdata.2017.88, 2017.

Penman, H. L.: Natural evaporation from open water, bare soil and grass, Proc. R. Soc. Lond. A, 193, 120–145, https://doi.org/10.1098/rspa.1948.0037, 1948.

Power, S., Casey, T., Folland, C., Colman, A., and Mehta, V.: Inter-decadal modulation of the impact of ENSO on Australia, Clim. Dynam., 15, 319–324, https://doi.org/10.1007/s003820050284, 1999.

Qin, M., Dai, A., Li, D., and Hua, W.: Understanding the inter-decadal variability of autumn precipitation over North Central China using model simulations, Int. J. Climatol., 40, 874–886, https://doi.org/10.1002/joc.6245, 2020.

Qin, M., Li, D., Dai, A., Hua, W., and Ma, H.: The influence of the Pacific Decadal Oscillation on North Central China precipitation during boreal autumn, Int. J. Climatol., 38, e821–e831, https://doi.org/10.1002/joc.5410, 2018.

Shi, J., Yan, Q., Jiang, D., Min, J., and Jiang, Y.: Precipitation variation over eastern

China and arid central Asia during the past millennium and its possible mechanism: Perspectives from PMIP3 experiments, J. Geophys. Res.-Atmos., 121, 11,989–12,004, https://doi.org/10.1002/2016JD025126, 2016.

Shi, J., Yan, Q., and Wang, H.: Timescale dependence of the relationship between the East Asian summer monsoon strength and precipitation over eastern China in the last millennium, Clim. Past, 14, 577–591, https://doi.org/10.5194/cp-14-577-2018, 2018.

Shi, Y., Shen, Y., Kang, E., Li, D., Ding, Y., Zhang, G., and Hu, R.: Recent and Future climate change in Northwest China, Climatic Change, 80, 379–393, https://doi.org/10.1007/s10584-006-9121-7, 2007.

Tardif, R., Hakim, G. J., Perkins, W. A., Horlick, K. A., Erb, M. P., Emile-Geay, J., Anderson, D. M., Steig, E. J., and Noone, D.: Last Millennium Reanalysis with an expanded proxy database and seasonal proxy modeling, Clim. Past, 15, 1251–1273, https://doi.org/10.5194/cp-15-1251-2019, 2019.

Turner, A. G. and Annamalai, H.: Climate change and the South Asian summer monsoon, Nat. Clim. Change, 2, 587–595, https://doi.org/10.1038/nclimate1495, 2012.

Wang, H. J.: The weakening of the Asian monsoon circulation after the end of 1970's, Adv. Atmos. Sci., 18, 376–386, https://doi.org/10.1007/BF02919316, 2001.

Wang, T. and Miao, J. P.: Twentieth-century Pacific Decadal Oscillation simulated by CMIP5 coupled models, Atmos. Ocean Sci. Lett., 11, 94–101, https://doi.org/10.1080/16742834.2017.1381548, 2018.

774 Wang, T., Wang, H. J., Otterå, O. H., Gao, Y. Q., Suo, L. L., Furevik, T., and Yu, L.:

775 Anthropogenic agent implicated as a prime driver of shift in precipitation in

776 eastern China in the late 1970s, Atmos. Chem. Phys., 13, 12433–12450,

777 https://doi.org/10.5194/acp-13-12433-2013, 2013.

778 Wang, T., Xu, H., Jiang, D., and Yao, J.: Mechanisms of reduced mid-Holocene

779 precipitation in arid Central Asia as simulated by PMIP3/4 models, J. Geophys.

780 Res.-Atmos., 127, e2021JD036153, https://doi.org/10.1029/2021JD036153,

781 2022.

782 Webster, P. J. and Yang, S.: Monsoon and ENSO: Selectively interactive systems, Q. J.

783 Roy. Meteor. Soc., 118, 877–926, https://doi.org/10.1002/qj.49711850705, 1992.

784 Xu, H., Wang, T., Wang, H., Chen, S., and Chen, J.: External forcings caused the

785 tripole trend of Asian precipitation during the Holocene, J. Geophys.

786 Res.-Atmos., 128, e2023JD039460, https://doi.org/10.1029/2023JD039460,

787 2023.

788 Xu, H., Wang, T., Wang, H., Miao, J., Chen, J., and Chen, S.: The PMIP3 simulated

789 climate changes over arid Central Asia during the mid-Holocene and last glacial

790 maximum, Acta Geol. Sin.-Engl., 94, 725–742,

791 https://doi.org/10.1111/1755-6724.14542, 2020.

792 Xue, J., Ning, L., Liu, Z., Qin, Y., Chen, K., Yan, M., Liu, J., Wang, L., and Li, C.:

793 The combined influences of solar radiation and PDO on precipitation over

794 eastern China during the last millennium, Clim. Dynam., 60, 1137–1150,

795 https://doi.org/10.1007/s00382-022-06372-4, 2023.

Zhang, Y. and Huang, D.: Has the East Asian westerly jet experienced a poleward displacement in recent decades?, Adv. Atmos. Sci., 28, 1259–1265, https://doi.org/10.1007/s00376-011-9185-9, 2011.

Zhao, P., Yang, S., and Yu, R.: Long-term changes in rainfall over eastern China and large-scale atmospheric circulation associated with recent global warming, J. Climate, 23, 1544–1562, https://doi.org/10.1175/2009jcli2660.1, 2010.

Zhao, X., Dong, B., and Lu, R.: Interdecadal weakening of the cross-equatorial flows over the Maritime Continent during the boreal summer in the mid-1990s: drivers and physical processes, Clim. Dynam., 57, 55–72, https://doi.org/10.1007/s00382-021-05692-1, 2021.

Zhu, J., Zhao, K., Wang, Y., Cui, Y., Liang, Y., Cheng, H., Edwards, R. L., Kong, X., Shao, X., Chen, S., and Pang, L.: Decadal modulation of East Asian summer monsoon variations by external forcing and internal variability, Quaternary Sci. Rev., 293, 107720, https://doi.org/10.1016/j.quascirev.2022.107720, 2022.

Zhu, Y., Wang, H., Ma, J., Wang, T., and Sun, J.: Contribution of the phase transition of Pacific Decadal Oscillation to the late 1990s' shift in East China summer rainfall, J. Geophys. Res.-Atmos., 120, 8817–8827, https://doi.org/10.1002/2015JD023545, 2015.